Spiral Wave Generation in Heterogeneous Excitable Media

Gil Bub, Alvin Shrier, and Leon Glass

Department of Physiology, McGill University, 3655 Drummond Street, Montreal, Quebec, Canada H3G 1Y6
(Received 15 June 2001; published 16 January 2002)

As the coupling in a heterogeneous excitable medium is reduced, three different types of behavior are encountered: plane waves propagate without breaking up, plane waves break up into spiral waves, and plane waves block. We illustrate these phenomena in monolayers of chick embryonic heart cells using calcium sensitive fluorescent dyes. Following the addition of heptanol, an agent that reduces the electrical coupling between cells, we observe breakup of spiral waves. These results are modeled in a heterogeneous cellular automaton model in which the neighborhood of interaction is modified.

Excitable media, such as the Belousov-Zhabotinsky reaction, oxidation reactions on platinum surfaces, forest fires, or the heart, support propagating waves of constant amplitude in a variety of different geometrical patterns including plane waves, spirals, and multiple spirals. The stability of these waves depends on a number of factors including the properties of the medium and the presence of heterogeneities [1–7]. In order to investigate the relative roles of heterogeneity and coupling in the stability of waves in excitable medium, we study an experimental cardiac system in which it is possible to change the coupling experimentally and to compare the results with a cellular automaton model in which coupling is varied.

Tissue cultures of cardiac cells display a range of complex dynamics [8–10]. In the current work, we investigate the effects of lowering cell-cell connectivity on spiral waves imaged with optical mapping techniques in cultured monolayers of cardiac myocytes [11]. Cell-cell connectivity is lowered by heptanol, a pharmacological agent that inhibits conduction through specialized pores, called gap junctions, that connect cells [12].

Figure 1 shows the dynamics observed in embryonic chick heart cells using calcium sensitive fluorescent dye. In the control condition a double-armed spiral rotates with a period of 0.7 s with an approximate wave speed of 1.5 cm/s. Immediately after the addition of heptanol, the waves are blocked. They spontaneously reinitiate within 30–40 s. Slowly traveling waves immediately develop numerous breaks as they travel through the medium. Subsequent waves exhibit wave breaks at the same physical locations. The second row in Fig. 1 shows the situation 50 s after the addition of heptanol, when the wave speed is 0.2–0.4 cm/s. Multiple broken waves, originating from regions of block, evolve into several spiral waves with a period of about 0.75 s. Following washout of the heptanol, wave propagation that is qualitatively similar to control was reestablished. This experiment was repeated in eight different preparations and qualitatively similar results were found in all cases.

Several approaches have been developed to model the effects of heterogeneities in cardiac muscle. The models developed so far have simulated the effects on conduction of a small number of anatomical obstacles [5], single [6] and multiple [7] sites of electrophysiological heterogeneity, and regions with variability in cell refractoriness [2]. Our cell culture system has heterogeneities in cell density and connectivity distributed over the whole medium. We study a very simple cellular automaton modified from early proposals by Greenberg-Hastings [13] that we believe captures the effects of a heterogeneous cellular structure.

The Greenberg-Hastings model is formulated as follows. Each site at time (t) is assigned a state, $u_j(t)$, where the subscript refers to the cell number. The neighborhood of a given site is determined using a square (Moore) metric. The state is an integer: 0 is a rest state; states $1, 2, \ldots, E$ are excited states; states $E + 1, E + 2, \ldots, E + R$ are refractory states; state $(E + R + 1)$ is identified with the rest state 0. The update rule for the state of a site is as follows: if $1 \leq u_i(t) \leq (E + R)$, then $u_i(t + 1) = u_i(t) + 1$. If $u_i(t) = 0$, then $u_i(t + 1) = 0$, unless u_i is excited by its neighbors. In the original Greenberg-Hastings model all
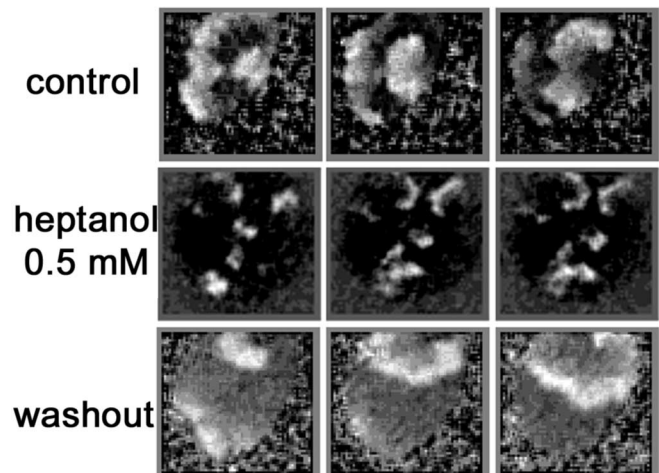

FIG. 1. Effects of heptanol on excitation in embryonic chick heart cells visualized with calcium sensitive fluorescent dye. Each box is approximately 0.6 cm². Each row shows three consecutive images at 200 ms intervals. We show the patterns before heptanol addition (top row), 50 s after heptanol addition (middle row), and 60 s after heptanol washout (bottom row).

cells were on a square lattice. A cell would be excited if a sufficient number of excited cells is present in a defined neighborhood around the cell.

We introduce spatial heterogeneity in the cell density by perturbing the location of each cell [14]. We take the nearest neighbor distance between cells to be 1. Given the original coordinates (x_0, y_0), the new coordinates are $(x_0 + \epsilon_x, y_0 + \epsilon_y)$, where ϵ_x, ϵ_y are uniformly distributed in the interval $[-0.5, 0.5]$. We also assign a random weight for a cell's influence on its neighbors. Each cell is assigned a random weight, S_i, uniformly distributed in the range $0.5 < S_i < 1.5$ [15].

The condition for an unexcited cell i to become excited is as follows. If $u_i(t) = 0$, then $u_i(t + 1) = 1$ if

$$\frac{\sum_{D[j,i]<r;0<u_j(t)\leq E} S_j}{\sum_{D[j,i]<r;u_j(t)=0 \text{ or } u_j(t)>E} S_j} > \theta, \qquad (1)$$

where $D[j,i] = |x_j - x_i| + |y_j - y_i|$ is the distance between cell j and cell i, (x_j, y_j) is the location of cell j, θ is the excitation threshold, and the summation is over all cells within a distance r of cell i. In this formulation, excitation is not determined only by the excited cells in the neighborhood of a given cell, but by the ratio of excited to nonexcited cells in the neighborhood of a given cell. Equation (1) allows the model to simulate the effects of current sinks that affect propagation in cardiac systems [8,16]. The addition of heptanol is modeled by reducing r. Simulations were carried out in an array of 600×600 cells with the cells in the top four rows being excited at $t = 0$ with $E = 12$, $R = 13$.

For a fixed value of θ, different dynamic regimes are observed as r increases. The different behaviors as a function of r can be appreciated from Fig. 2. The different rows in Fig. 2 show the dynamics for different values of r. Column (a) shows all the cells that have ever been active (grey) compared to the cells that have never been active (black) after 100 iterations. Column (b) shows the activity after 100 iterations (active cells are white, refractory cells are grey, and inactive cells are black). Column (c) shows the activity after 1000 iterations when transients have died out. For low values of r propagation is blocked, for intermediate values of r spirals are initiated locally and evolve to dominate the dynamics, and for large values of r the plane wave propagates without the generation of spirals so that after 1000 iterations there is no more activity in the network.

The first column of Fig. 2 shows that as the value of r increases, the boundary separating the excited cells and the excitable cells becomes increasingly smooth, and the velocity increases. This suggests the following mean field approach. Assume the boundary is smooth, and consider an unexcited cell a distance δ away from the boundary. The area in the neighborhood of the cell which is excited is $2r(r - \delta)$ and the area which is not excited is $2r(r + \delta)$ (the distance metric we use makes these expressions trans-
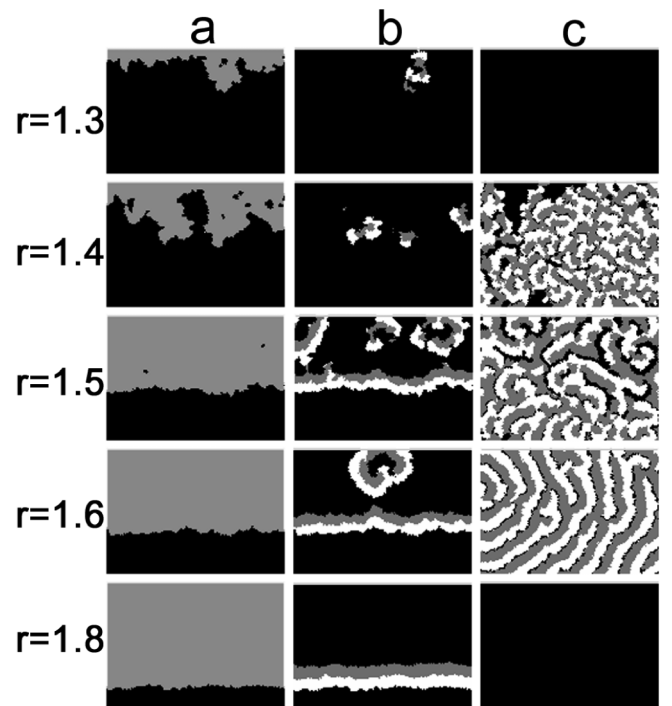

FIG. 2. Dynamics in the modified Greenberg-Hastings model with $\theta = 0.35$. Each row represents a different value of r. A plane wave is started at the top of the system. Each panel represents an array 150 cells wide and 100 cells high. Column (a): All the cells that have ever been active (grey) compared to the cells that have never been active (black) after 100 iterations. Column (b): The activity after 100 iterations (active cells are white, refractory cells are grey, and inactive cells are black). Column (c): The activity after 1000 iterations when transients have died out.

parent, but other metrics give qualitatively similar dynamics). Since the mean weight of each of the inputs to the cell is 1, the condition for a cell to be excited is

$$\frac{r - \delta}{r + \delta} > \theta. \qquad (2)$$

Consequently, the distance of the propagation per iteration for the situation when the wave front is smooth is given by

$$\delta = \frac{r(1 - \theta)}{1 + \theta}. \qquad (3)$$

Figure 3 plots the velocity, v, as a function of r [17] for three values of θ and compares this with the estimates from Eq. (3). For sufficiently large values of r, there is excellent agreement, but as r decreases propagation slows and then fails. This is associated with a roughening of the wave front so that the mean field approximation used to derive Eq. (3) is no longer valid.

To further analyze the failure of propagation, in Fig. 4(a) we show the regions of blocked propagation (B), spiral formation (S), and plane wave propagation (P) as a function of r for $\theta = 0.35$.

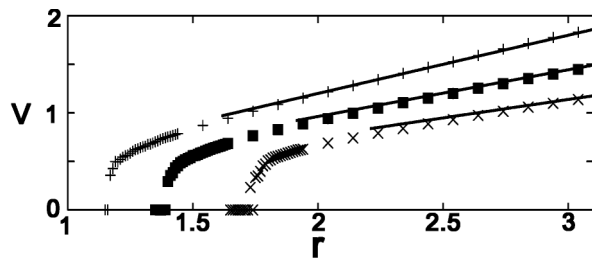As θ increases the left-hand boundary of the spiral forming region increases as shown in Fig. 4(b). Referring to

FIG. 3. The velocity of propagation as a function of r for $\theta = 0.25$ (+), $\theta = 0.35$ (square), and $\theta = 45$ (×) compared with the results from Eq. (3) (solid lines).

Eq. (2), we assume that propagation will fail at a critical distance r_c, when the mean distance of a cell from the wave front is δ_c. From this we compute

$$r_c = \frac{\delta_c(1 + \theta)}{(1 - \theta)}. \qquad (4)$$

Since the propagating wave front is extremely rough for parameter values that are near the boundary where propagation fails, the above expression is approximate and we choose to treat δ_c as an adjustable parameter. If we assume $\delta_c = 0.67$ we find quantitative agreement between the value of r_c from Eq. (4) and the numerically computed value, Fig. 4(b). The analytic computation of the boundary separating the region of blocked propagation and the spiral initiating region in Fig. 4(a) represents a challenge. In the course of this work, we implemented many different models including heterogeneous cellular automata with fixed thresholds and continuous coupled partial differential equations with randomly dispersed missing lattice
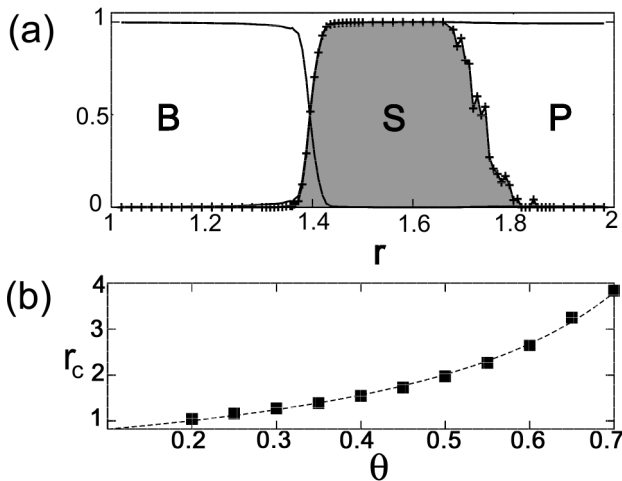

FIG. 4. Dynamics of propagation block. (a) The fraction cells that are excited in a window of 100 iterations averaged over 20 different arrays following a transient of 3000 iterations for $\theta = 0.35$ is the shaded region labeled S. The solid curve defining the blocked region (B) is defined by the fraction cells that never get excited and the solid curve defining the propagating region labeled P is defined by the fraction of cells that do get excited. (b) r_c in the simulations is the value of r where 50% of the cells have been activated (squares). This is compared with r_c, from Eq. (4) with $\delta_c = 0.67$.

058101-3

sites. Since the discrete cellular automaton without heterogeneity does not exhibit breakup of the propagating waves, and the continuous model with heterogeneity does exhibit breakup of propagating waves, we believe that the heterogeneity rather than the discreteness is the crucial feature. Further, in contrast to previous models [2], the heterogeneity is not in the refractory time, but rather in the coupling of the cells.

The current work has implications for understanding the onset and maintenance of complex abnormal cardiac rhythms. Although, cardiologists have long believed that heterogeneities play an essential role in the initiation of serious arrhythmias in diseased hearts [2], in normal heart muscle many heterogeneities occur at comparatively small space scales so that homogeneous equations offer a good approximation to the dynamics [18]. However, this generalization is not valid in disease states where cell connectivity and propagation velocity are greatly reduced [19,20] and continuous models of cardiac tissue may not be valid. With reduced coupling, propagation direction and stability are affected by local asymmetries in cell spacing and connectivity [8,21,22]. Our observations may be relevant to the onset and evolution of spiral waves observed in ventricular fibrillation, a cardiac arrhythmia that is often encountered in situations in which cell coupling is compromised [23].

The origin of spiral waves and the breakup of spiral waves in natural systems is not clear. Although theoretical models of homogeneous discrete [3] and continuous [4] excitable media can show breakup of spiral waves even in the absence of heterogeneities, in natural systems it is difficult to eliminate heterogeneity. There are interactions between heterogeneity and excitability, and it should be of interest to study natural and model systems in which both of these factors can be independently varied. In the current work, we have kept the heterogeneity fixed as the coupling was varied. As coupling varies in a heterogeneous excitable media, one goes from a system that does not support wave propagation to a system in which plane waves propagate. For intermediate parameter values, plane waves break up into multiple spiral waves.

[1] K. Chen, P. Bak, and M. H. Jensen, Phys. Lett. A **149**, 207 (1990); J. Maselko and K. Showalter, Physica (Amsterdam) **49D**, 21 (1991); K. Agladze, J. P. Keener, S. C. Muller, and A. V. Panfilov, Science **264**, 1746 (1994); R. Imbihl and G. Ertl, Chem. Rev. **95**, 697 (1995); M. Bar et al., J. Phys. Chem. **100**, 19 106 (1996); I. Sendina-Nadal et al., Phys. Rev. E **58**, 1183 (1998); I. Schebesch and H. Engel, Phys. Rev. E **57**, 3905 (1998); S. Clar et al.,

Physica (Amsterdam) **266A**, 153 (1999); F. Xie, Z. Qu, J. N. Weiss, and A. Garfinkel, Phys. Rev. E **63**, 031905 (2001).

[2] G. K. Moe, W. C. Rheinboldt, and J. A. Abildskov, Am. Heart J. **67**, 200 (1964); J. M. Smith and R. J. Cohen, Proc. Natl. Acad. Sci. U.S.A. **81**, 233 (1984); A. Bardou, S. Achour, P. Auger, and J. L. Chasse, Int. J. Bifurcation Chaos **6**, 1657 (1996).

[3] H. Ito and L. Glass, Phys. Rev. Lett. **66**, 671 (1991).

[4] A. Karma, Phys. Rev. Lett. **71**, 1103 (1993).

[5] J. M. Starobin, Y. I. Zilberter, E. M. Rusnak, and C. F. Starmer, Biophys. J. **70**, 581 (1996).

[6] A. Xu and M. R. Guevara, Chaos **8**, 157 (1998).

[7] F. Xie, Z. Qu, A. Garfinkel, and J. N. Weiss, Am. J. Physiol. Heart Circ. Physiol. **280**, H535 (2001).

[8] S. Rohr, J. P. Kucera, V. G. Fast, and A. G. Kleber, Science **275**, 841 (1997).

[9] G. Bub, L. Glass, N. G. Publicover, and A. Shrier, Proc. Natl. Acad. Sci. U.S.A. **95**, 10 283 (1998).

[10] Y. Soen, N. Cohen, D. Lipson, and E. Braun, Phys. Rev. Lett. **82**, 3556 (1999).

[11] We map excitation waves in monolayers of embryonic cardiac tissue using a macroscope imaging system [9]. Culture: Monolayers of seven-day embryonic chick ventricular myocytes cultured for $48-72$ h at just under confluent densities $[(7.0-14.0) \times 10^3$ cells/cm$^2]$ yielding randomly oriented cells [9]. Cells were plated within a 12 mm diameter glass retaining ring on lysine-coated plastic cell culture dishes. Monolayers at this age display stably rotating spiral waves or regularly firing targets. Monolayers display bursting dynamics [9] when incubated for shorter $(24-36$ h) times. Cells were kept in maintenance medium 818a at 5% CO_2 at 36 °C before experiments. Monolayers were loaded with calcium sensitive dye Fluo-3-AM (5 μM, 30 min) in Tyrode (1.3 mM K) for 25 min, then transferred to the imaging setup. Imaging: The optical mapping system was described in previous publications [9]. A macroscope was constructed to allow low light level measurements at low magnification scales (objective: Nikon 80 mm, imaging lens Chromicar Zoom 130, excitation filter, 460 nm, dichroic beam splitter at 510, imaging filter 540, Omega optical). The macroscope was mounted on top of an inverted microscope (Zeiss Axiovert 125M) to allow for simultaneous monitoring of the monolayer at macroscopic and microscopic scales. Images were collected using a cooled charge-coupled device (CCD) camera (Princeton Instruments, Model TE CCD 576). Adjacent pixels in the CCD were binned (2×2) and up to 30 000 consecutive images were transferred directly to a computer (Pentium) for storage and analysis. Image data from each binned pixel is scaled based on its maximal range over 20 frames, and the image is spatially averaged, background subtracted, and viewed using custom-written software. Calcium sensitive dyes are used to allow long recording times with high signal to noise ratios while minimizing phototoxic damage. Calcium can reliably be used as a surrogate for direct voltage measurement in our system. We have confirmed this by measuring optical records of preparations loaded with voltage sensitive dye and calcium sensitive dye. These movies are available on-line at www.cnd.mcgill.ca/bios/bub/movies.html. The experiments presented in this Letter map excitation using Ca^{++} sensitive dye fluorescence.

[12] H. Kimura et al., Exp. Cell Res. **220**, 348 (1995).

[13] J. Greenberg, B. Hassard, and S. Hastings, SIAM J. Appl. Math. **34**, 515 (1978); M. Gerhardt, H. Schuster, and J. J. Tyson, Science **247**, 1563 (1990); R. Fisch, J. Gravner, and D. Griffeath, Stat Computing **1**, 23 (1991).

[14] M. Markus and B. Hess, Nature (London) **347**, 56 (1990).

[15] The results are qualitatively the same for constant S_i. However, if each weight S_i is a whole number, the values of r where propagation fails cluster around the square root of whole numbers. Incorporating random values for S_i is a simple way to introduce a continuously varying number of neighbors with varying r.

[16] C. Delgado et al., Circ. Res. **67**, 97 (1990); Y. Wang and Y. Rudy, Am. J. Physiol. **278**, H1019 (2000).

[17] The velocity is the average propagation distance per iterate determined from the first iteration that leads to an excitation in the 600th row.

[18] L. Clerc, J. Physiol. (London) **255**, 335 (1976); M. S. Spach et al., Circ. Res. **48**, 39 (1981); M. S. Spach, Int. J. Bifurcation Chaos **6**, 1637 (1996); A. T. Winfree, Int. J. Bifurcation Chaos **7**, 487 (1997); A. T. Winfree, *When Time Breaks Down: The Three-Dimensional Dynamics of Electrochemical Waves and Cardiac Arrhythmias* (Princeton University Press, Princeton, NJ, 1987).

[19] R. W. Joyner et al., Biophys. J. **71**, 237 (1996); R. M. Shaw and Y. Rudy, Circ. Res. **81**, 727 (1997).

[20] J. M. de Bakker et al., Circulation **77**, 589 (1998); H. J. Jongsma and R. Wilders, Circ. Res. **86**, 1193 (2000); A. Arutunyan, D. R. Webster, L. M. Swift, and N. Sarvazyan, Am. J. Physiol. Heart Circ. Physiol. **280**, H1905 (2001).

[21] R. W. Joyner, Biophys. J. **35**, 112 (1981); R. W. Joyner, R. Veenstra, D. Rawling, and A. Chorro *ibid.* **45**, 1017 (1984).

[22] S. Rohr, J. P. Kucera, and A. G. Kleber, Circ. Res. **83**, 781 (1998); J. P. Kucera, A. G. Kleber, and S. Rohr *ibid.* **83**, 795 (1998).

[23] C. J. Wiggers, Am. Heart J. **20**, 399 (1940); F. X. Witkowski et al., Nature (London) **392**, 78 (1998).